Iranian Journal of Materials Forming 10 (3) (2023) 15-24

Online ISSN: 2383-0042

Iranian Journal of Materials Forming

Journal Homepage: http://ijmf.shirazu.ac.ir

Research Article

Numerical Simulation and Evaluation of Effective Parameters During Cold Drawing of 410 Stainless Steel Tubes

M.M. Niazi[1], E.M. Sharifi[1], R. Vafaei[1], A. Mahdian[2*]

[1]Department of Materials Engineering, Malek Ashtar University of Technology, Isfahan, Shahin Shahr, Iran
[2]Department of Mechanical Engineering, Malek Ashtar University of Technology, Isfahan, Shahin Shahr, Iran

ARTICLE INFO

Article history:

Received 04 August 2023
Reviewed 09 September 2023
Revised 18 October 2023
Accepted 20 October 2023

Keywords:

Simulation
410 stainless steel
Drawing force
Friction
Die angle

Please cite this article as:

M.M. Niazi, E.M. Sharifi, R. Vafaei, A. Mahdian, Numerical Simulation and Evaluation of Effective Parameters During Cold Drawing of 410 Stainless Steel Tubes, *Iranian Journal of Materials Forming*, 10 (3) (2023) 15-24.

ABSTRACT

This study evaluates the effects of the changing die angles on drawing force during cold drawing of a 410 stainless steel tube. For this purpose, a simulation of the process by the Abaqus software was performed and the results were compared with the experimental findings. By applying Johnson and Cook's equation the flow behavior of the steel was also assessed during cold drawing. Ring compression tests were performed to determine the coefficient of friction at die-tube and tube-plug interfaces. Furthermore, strain distribution during the process was considered to evaluate the mechanical behavior of the steel. An essential aspect of the work was to estimate the required drawing force, by lower and upper-bound theories. It is illustrated that the lowest drawing force is obtained at the half-die angle of 16°. At this angle a drawing force of 164.6 kN was estimated by simulation. Experimental results at the half-die angle of 16° indicated a drawing force of 175.1 kN which illustrates about 5% discrepancy with simulated results. In addition, the radial strains at this die angle had the highest value in comparison with the other half-die angles of 12 and 14 degrees. The highest amount of strain was observed in the axial direction of the drawing process at the half-die angle of 16°. The lowest values of residual stresses were developed at this die angle.

1. Introduction

Stainless steel tubes are widely used in petroleum, nuclear, and gas industries. The austenitic and martensitic types are usually used to manufacture heat exchangers and alike materials. Martensitic stainless steels are considered to have high hardness and strength, good fatigue behavior, resistant to wear and corrosion. Cold tube drawing is one of the important methods of manufacturing tubes of such steels with high dimensional accuracy and good surface finish, which is escorted with improved mechanical properties. The process involves passing a feedstock tube through a die, with or without an internal plug or mandrel. Internal tools are critical for controlling the size of the inner diameter and the surface integrity [1].

To attain the final dimensions, the tubes are reduced in diameter and wall thickness by several drawing steps.

* Corresponding author
E-mail address: m.mehdi.niazi@gmail.com (M.M. Niazi)
https://doi.org/10.22099/IJMF.2023. 48020.1266

Performing intermediate annealing is also necessary. However, several parameters influence the flow behavior of the material and the required drawing force. For example, friction at the interface of dies and the material play a major role on the final shape and the required drawing force. Usually, solutions of soap and oil are used for lubrication during cold drawing processes [2, 3]. Nevertheless, the choice of appropriate die angle is a key factor which influences the drawing force, redundant strains, frictional forces and residual stresses in the final product. The amount of required force is also affected by chemical composition and mechanical properties of the feedstock as well as the volume reduction of cross-section. The expected value of drawing force can be theoretically calculated by utilizing upper bound analysis. However, numerical simulation methods are among the most effective methods for predicting the amount of required tensile force [1, 4]. Numerous studies based on numerical simulations and experimental tests is carried out to determine the effective parameters on cold drawing. Chobaut et al. [5] studied the effects of friction coefficient and tensile limit of SS 316L tube via FEM and found that changing the type of lubricant and preheating feed stock can decrease the friction coefficient and required force. Palengat et al. [6] also evaluated the effects of temperature and friction by using experimental tests and inverse analysis on the drawing of 316L stainless steel tubes and showed that force values were correctly predicted. Linadron [7] determined the tensile load and ultimate tensile strength of L605 and 316LVM materials in tube drawing. It was indicated that lowering the die angle results in increasing the principal stresses. A decrease in the die angle caused higher compressive stresses. Moreover, the energy dissipated by friction decreased by increasing the die angle, while the energy dissipated by plastic deformation increased by rising it. Boutnel et al. [8] investigated the influence of the die angle on the drawing force and thickness ratio on a tensile load via simulation on a 316LVM tube. It was shown that relative thickness has an effect on the mechanical behavior of the tube. Nekpal et al. [9] used axial-symmetric Lagrangian formulation on a SPT360 and compared the parameters of plastic deformation obtained experimentally by measuring microstructural characteristics of oriented grains with data obtained from FEM simulation. By Considering tools as rigid and forming material as plastic, it was shown that the power law definition appears to be sufficient for the simulation of cold drawing processes. Gattmah et al. [10] investigated the effects of semi-die/plug angles on drawing stress for different friction coefficients in 1010 steel tubes and showed the effects of semi-die angle on plastic deformation. Semi-die angle of 12° gave minimum drawing stress for all coefficient of frictions. Beland et al. [11] worked on optimization of the tool geometry by using the finite element method to reduce the maximum stress level for tubes of Al6063 in one pass. It was shown that minimizing axial stress makes it possible to reduce the production cycle from two stages to one. Keun et al. [12] by using a fixed plug, applied an upper bound solution for calculating the required tensile stress during tube drawing. They showed that optimum semi-die angle minimizes the drawing stress.

Given that there is very limited data on the effect of cold drawing on martensitic stainless-steel tubes, the current research is focused on providing practical data in this regard. The aim is to use the finite element method (FEM) to evaluate and predict the minimum drawing force on the cold drawing process of a 410 martensitic stainless-steel tube. Additionally, the effect of varying die angles during drawing was investigated in order to obtain the optimum drawing force.

Different methods including numerical simulation with Abaqus software, upper and lower bound analysis and the experimental cold drawing process were used to compare and validate the results. Although, no load cell was used in the practical drawing experiments but the drawing force was estimated from the current consumption of the electric motor of drawing bench. In addition, using different lubricants, the coefficient of friction between the die and the tube was recognized by the ring test method and a suitable lubricant was introduced.

2. Experimental Procedure

2.1. Sample preparation and test plan

An Annealed AISI 410 steel with the chemical composition and mechanical properties tabulated in table 1 was used in this research. The tube had an outer diameter of 34 mm with a thickness of 3 mm and was drawn using a fixed plug and a 30 tons drawing machine. The tube drawing was carried out in two steps; the first stage reducing the cross-sectional area by 26% down to 29*2.6 mm^2 followed by an intermediate annealing. In the second step, the section area was reduced by 28.4% to the final size of 25.4*2.11 mm^2. The die used in the first step had a diameter of 29 mm, a half angle of 16°, and a bearing area of 5 mm^2. In the second step, the die used had a diameter of 25.4 mm, a half angle of 16° and a bearing area of 5 mm^2. A cylindrical plug with a diameter of 23.8 mm was used to keep the internal diameter unchanged. The tubes were drawn at different speeds of 5, 10, and 15 mm/min. The coefficient of friction was estimated by the Ring Compression Test (RCT) using samples with outer and inner diameters of 30 and 15 mm, respectively. The thickness of rings was taken as 10 mm (6:3:2 ratio). The tests were carried out on a 100-tons press machine. Finally, two types of lubricants, including a hot solution of oxalate and soap and drawing oil of the type Lub 7000, were used to determine the appropriate coefficient of friction for the experiments.

Table 1. Chemical composition and mechanical properties of 410 stainless steel tube

Chemical composition (wt. %)							
Mo	Ni	Cr	P	S	Mn	Si	C
0.02	0.27	13.1	0.029	0.005	0.39	0.33	0.07

Mechanical properties					
Density (kg/m^3)	Poisson's ratio	Young modulus (GPa)	Hardness (Hv)	Yield strength (MPa)	Ultimate strength (MPa)
7700	0.3	200	142	469	524

2.2. Determination of the experimental drawing force

As shown in Fig. 1, the experimental drawing process was carried out on an industrial drawing bench.

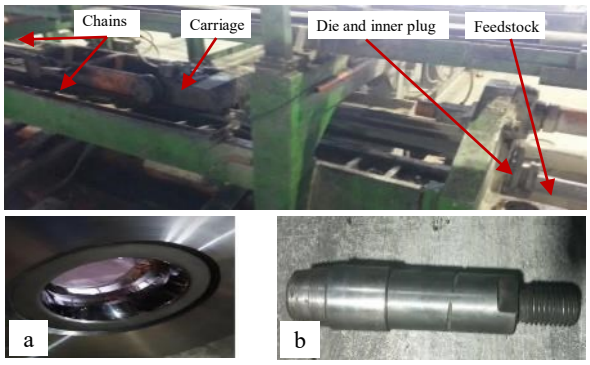

Fig. 1. 30 tons industrial drawing bench (a) The die and (b) the plug used in this work.

The driving force of the machine was through a chain wheel with a diameter of 20 cm. A chain connected to a small carriage attached to a pair of jaws, pulls the tube through the die. The pulling force is calculated via an applied torque of the rotating motor of the draw bench illustrated as follows [13].

$$T_m = \frac{P}{\omega} = \frac{V.I\ \cos\varphi}{\omega} \quad (1)$$

Where P, T_m, ω,V and I, are the nominal power of electric motor (W), output torque (N.m) and angular velocity of output shaft of the motor (rad/s), voltage (V) and electric current (A), respectively. The power factor is $\cos\varphi$ = 0.8. The resulting force F (N) acting on jaws of the machine can be calculated through the following equation [13].

2.3. Simulation of the drawing process

Tube drawing simulation of the steel was carried out as a 200 mm long axisymmetric model by Abaqus 6.14 software. This was in accordance with experimental specimen size. Surface-to-surface contact between tools and the tube was used to express the boundary conditions. Columbic friction conditions were considered as tangential behavior at contact interfaces. Die and plug were taken as fixed without any degrees of freedom and the axial direction for the tube was one degree of freedom. Die angles of 12, 14, and 16 degrees were considered for the model, with the contact length of 5 mm. Also, a cylindrical model was assumed for the

plug as shown in Fig. 2 (a). Both plug and the die were taken as rigid, and 4XRT mesh type was applied for analysis of the simulation. Fig. 2 (b) illustrates the mesh convergence of the process with respect to the applied force. The material was assumed to be isotropic and tensile test results was used to determine the plastic flow stress behavior. As shown by relations of 3, 4 and 5, Johnson-Cook equation was applied to evaluate the material's behavior during the drawing process [14].

$$\sigma_y(\varepsilon_p.\dot{\varepsilon}_p.T) = [A + B(\varepsilon_p)^n][1 + C\ln(\dot{\varepsilon}_p{}^*)][1 - (T^*)^m] \quad (2)$$

$$\dot{\varepsilon}_p{}^* = \frac{\dot{\varepsilon}_p}{\dot{\varepsilon}_{p0}} \quad (3)$$

$$T^* = \frac{T - T_r}{T_m - T_r} \quad (4)$$

Where ε_p, $\dot{\varepsilon}_p$ are equivalent plastic strain and strain rate, respectively, and A, B, C, n, and m are the material's constants. Also, $\dot{\varepsilon}_p{}^*$ and T^* are normalized strain rate and temperature. (equations 4, 5). These parameters were calculated according to the tensile test results by drawing the exponential curve of true stress - strain at different strain rates of 0.1, 0.2, 0.4 s^{-1} and Cross head velocities of 5, 10, and 20 mm/min. Tensile samples were prepared according to ASTM A370 standard. The tests were carried out at constant speed of 5 mm/min, and the strain rate was calculated based on equation 6. The gauge length was taken as 50 mm [14].

$$\dot{\varepsilon}_{p0} = \frac{d\varepsilon}{dt} = \frac{\frac{dL}{L}}{dt} = \frac{1}{L}\frac{dL}{dt} = \frac{V}{L} = 0.1\ (1/s) \quad (5)$$

Fig. 3 depicts engineering stress-strain diagram of the raw material in the uniaxial tensile test. The yield strength is A=469 MPa. Work hardening constant is B=750 MPa and n=0.388 [14]. According to the measured values of elemental strains in the axial direction, the maximum amount of strain during the simulation is 10. Other Johnson–Cook parameters such as c=0.02 were calculated similar to Limbadri [14]. Due to the negligible effect of temperature, $T \approx T_r$ and T^*can be disregarded [14,15]. The simulation was conducted for half die angles (α) of 12, 14 and 16 degrees and the drawing force was predicted via FEM.

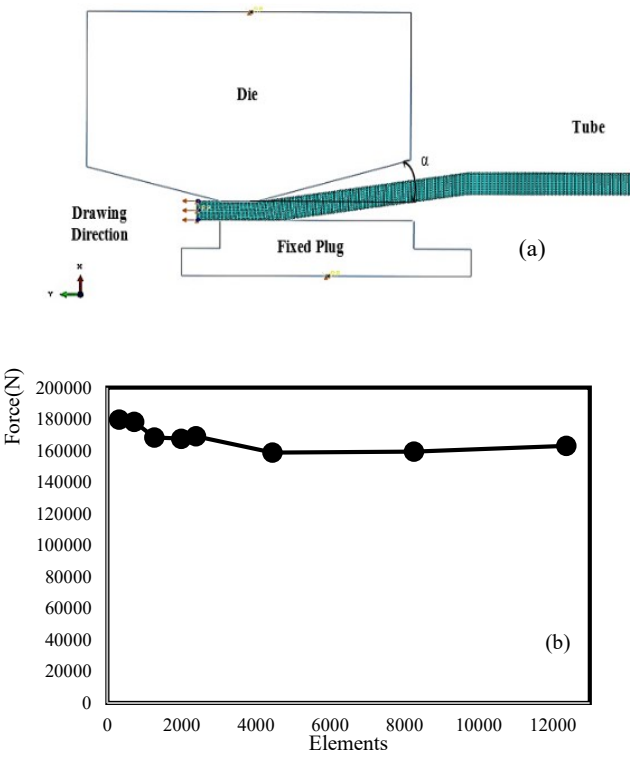

Fig. 2. (a) The cold drawing schematic, and (b) the mesh convergence of the process.

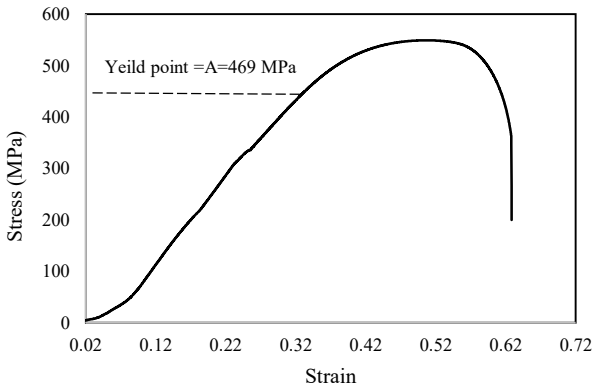

Fig. 3. Engineering stress-strain diagram of the raw material.

2.4. Lower bound and upper bound approaches

Upon calculating the required force via lower and upper bound theories, equation 7 was used. The accuracy of the calculated force is assessed by the FEM approach. The upper bound equation used is as follows [12].

$$\sigma_d = \frac{2\sigma_y}{\sqrt{3}}(1+x+x^2)^{\frac{1}{2}}\ln\frac{A_0}{A_f} + \frac{2\sigma_y}{3\sqrt{3}}\tan\alpha\left[\frac{R_0^2+R_0r_0+r_0^2}{R_0(R_0+r_0)}+\frac{R_f^2+R_fr_f+r_f^2}{R_f(R_f+r_f)}\right] + \frac{2\tau_i^{\alpha}}{\sin 2\alpha}\left[\frac{1}{1+t}\ln\frac{R_0+R_0t-R_ft+r_f}{R_f-r_f}+\frac{1}{1-t}\ln\frac{R_0+R_0t-R_ft+r_f}{R_f-r_f}\right] + \frac{2\tau_i^{\beta}}{\sin 2\beta}\left[\frac{-1}{1+t}\ln\frac{R_ft-r_f+r_0+r_0t}{(R_f-r_f)t}+\frac{1}{1-t}\ln\frac{R_ft-r_f+r_0+r_0t}{(R_f-r_f)t}\right] \quad (7)$$

$$x = \frac{d\varepsilon_\theta}{d\varepsilon_1} = \ln\frac{R_f+r_f}{R_0+r_0} / \ln\frac{R_0^2-r_0^2}{R_f^2-r_f^2} \quad (8)$$

Where X represents the ratio of circumferential to axial strain. R_0, R_f, r_0 and r_f show the initial outer radius, final outer radius, initial inner radius, and the final inner radius, respectively. Also, $\tau_i^{\alpha} = m^{\alpha}k$, $\tau_i^{\beta} = m^{\beta}k$ and $t = {\tan\beta}/{\tan\alpha}$. Since the plug is cylindrical (plug angle, β=0), τ_i^{β} can be considered 0.

The minimum required drawing stress was determined using slab analysis as the lower bound method (equation 9). In equation 10, $\beta = 0$ due to the use of cylindrical plug.

$$\frac{\sigma_d}{2k} = \frac{1+B}{B}\left[1-\left(\frac{t_f}{t_0}\right)^B\right] \quad (9)$$

$$B = \frac{\mu_1+\mu_2}{tg\alpha - tg\beta} \quad (10)$$

In equations 9 and 10, σ_d is the drawing stress, shear yield stress k is calculated from $2k=1.15\sigma_y$, B is related to the friction effects of half die angle and plug angle, t_f is the tube thickness after drawing, t_0 is the initial thickness of the tube, μ_1 and μ_2 represent the tube/die and plug/tube friction coefficients, respectively, and α and β are the half die angle and plug angle, respectively. [16].

3. Results and Discussion

As mentioned, the ring test was used to obtain the friction coefficient. The reduction in height of the rings was calculated according to the lessening of the inner diameter after the test [17]. However, by interpolating the results with the standard diagram, the average friction coefficient was estimated to be 0.15. Following the ring compression test, the sample's height and internal diameter were measured and the average friction coefficient was calculated using the standard chart of Fig. 4. As shown in Fig. 4, the average friction coefficient obtained for the oxalate-based lubricant was less than the drawing oil. Since the plug and the die were made of the same material, it was assumed that friction coefficients against the tube were identical. When the lubricants were changed to oxalate and soap solution, the tubes were drawn with no defects. However, cold drawing of the 410 steel with oil raised the friction leading to the rupture of the tube. Given the values obtained from the tensile test, the effects of different parameters on flow stress can be considered during the cold drawing process. Due to the small temperature change resulting from material deformation, temperature effects can be ignored. The Johnson-Cook equation for the drawing of the tube was obtained as follows:

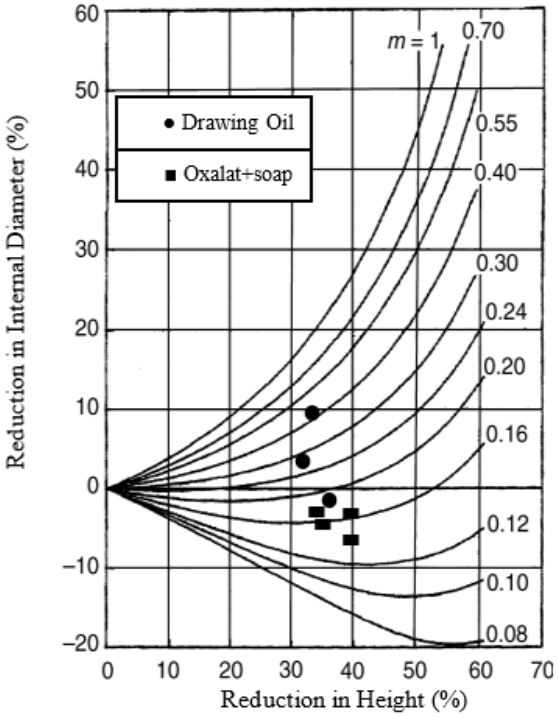

Fig. 4. Interpolating in the standard diagram [18].

$$\sigma_y(\varepsilon_p.\dot{\varepsilon}_p.T) = \left[469+750(\varepsilon_p)^{0.39}\right]\left[1+0.02\ln(\dot{\varepsilon}_p^{*})\right] \quad (11)$$

This equation describes the deformation behavior of 410 stainless steel during the cold drawing process at different strain and strain rates.

3.1. FEM Analysis

An overview of the simulated model for the cold

drawing process of 410 stainless steel is depicted in Fig. 1. In this layout, the tube is located in the dies, with the plug being inside the tube. Dynamic Explicit solution was utilized for performing the simulation. The plug had no longitudinal movement and the tube was drawn forward at a speed of 5 m/min (moderate speed of drawing bench). In mass scale investigation the ratio of kinetic energy to internal energy (KE/IE) for the mentioned model is 0 after almost 12 seconds. On the other hand, this value remained constant over time. It can be noticed that the kinetic energy is way lower than the internal energy (less than 1%). Hence, the results from the mass scaling are verified. The change in the force with the applied elements on the model is determined. The force decreases when the number of elements increase. However, when the number of elements increased beyond 4000, the force converged, indicating the suggested model was accurate enough. It should be mentioned that to verify the model, predicted results were compared with the experimental ones. Fig. 5 (a) shows the deformation of the tube through the die and the plug. It can be observed that the external and internal diameter of the tube decreases after the drawing process (Fig. 5); the applied deformation in the figure illustrates critical point at which maximum equivalent stresses act.

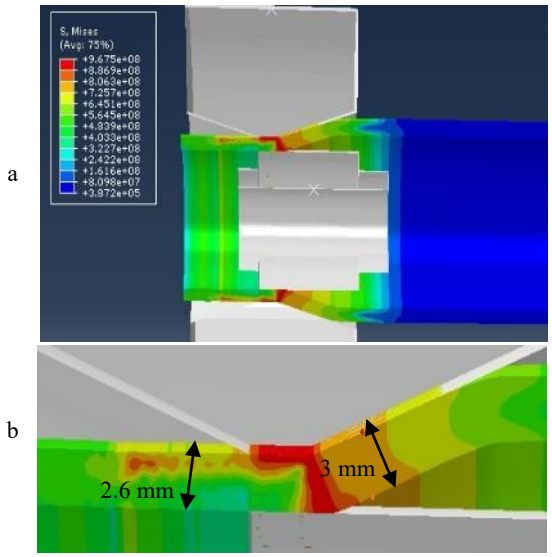

Fig. 5. (a) The initial moment of tube drawing and (b) the tube thickness before and after drawing.

The simulation results for half-die angles of 16, 14 and 12 are illustrated in Fig. 6 (a, b and c), respectively. The value of radial strain (ε_r) for the half die angle of 16 is higher than that of half angles of 12 and 14. The maximum and minimum radial strains for half-die angle of 16 was 0.0353 and -0.220, respectively, while for half-die angles of 14 and 12 are -3.96×10^{-5} and -0.199 -2.73×10^{-5} and –0.186, respectively. By comparing the results, it can be understood that the maximum axial strain for the three half-die angles are closely similar. Moreover, looking at the values obtained for the circumferential strains, the minimum compression strain for the half die-angle of 16 is -0.786×10^{-5}.

Fig. 7 shows the distribution of compressive and tensile strains created in the tube after the cold drawing process for the half die angle of 16°. According to Fig. 7 (a), it can be noticed that the tensile strain along the length of the tube is established as the process progresses. In other words, the value of the tensile strain at the start of drawing (colored blue in the figure), is approximately 0.04. With the progress of the process and further plastic deformation of the tube, the tensile strain at the end of the tube is approximately 0.44 (orange areas). It can also be seen in Fig. 7 (b), that the compressive strains follow the same path as the tensile strains during the drawing process. At the beginning of drawing (the part shown in red) the amount of compressive strain is very small (around - 0.022), While the amount of compressive strain at the end of the tube, colored indigo in Fig. 7 (b), is about -0.25.

Fig. 8 shows the changes in the values of radial, circumferential and axial strains on the internal and external surfaces, in the direction of the defined longitudinal path with a friction coefficient of 0.15. According to this figure, it can be seen that the strains on the inner and outer surfaces of the tube are almost equal. According to the obtained results, the axial and circumferential strains show the greatest effects on deformation. The circumferential strain had the lowest value during deformation, and its changes almost remained.

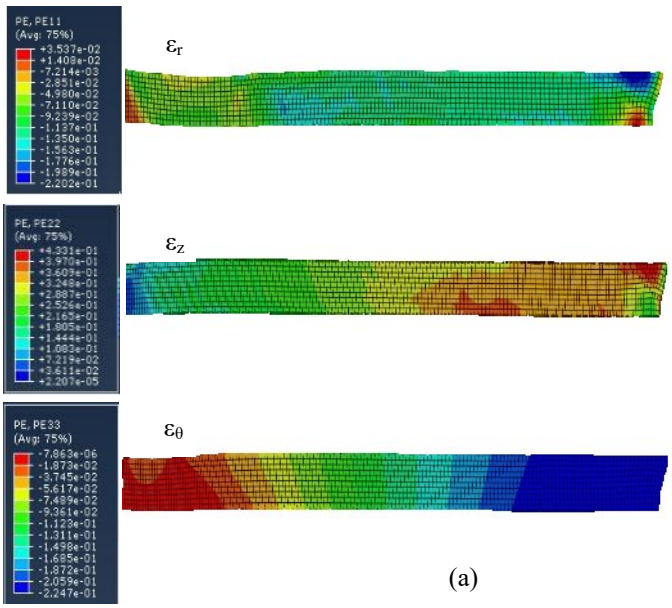

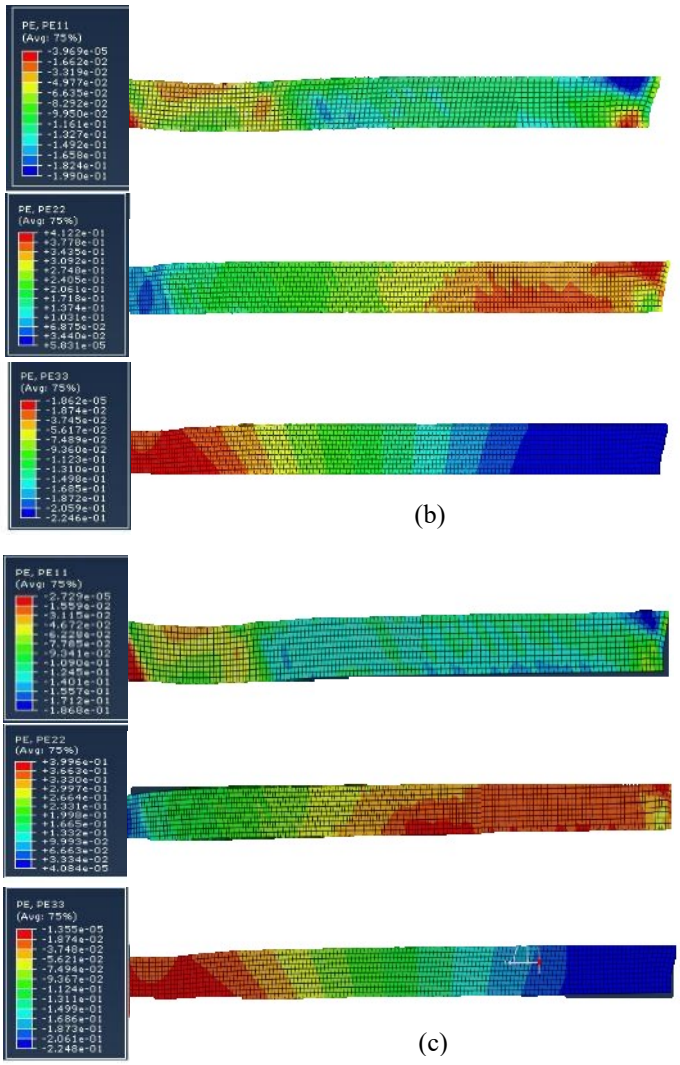

Fig. 6. Variations of radial ε_r, axial ε_z and circumferential ε_θ strains along the length of the drawn tube with a half angle of (a)16°, (b)14° and (c) 12°.

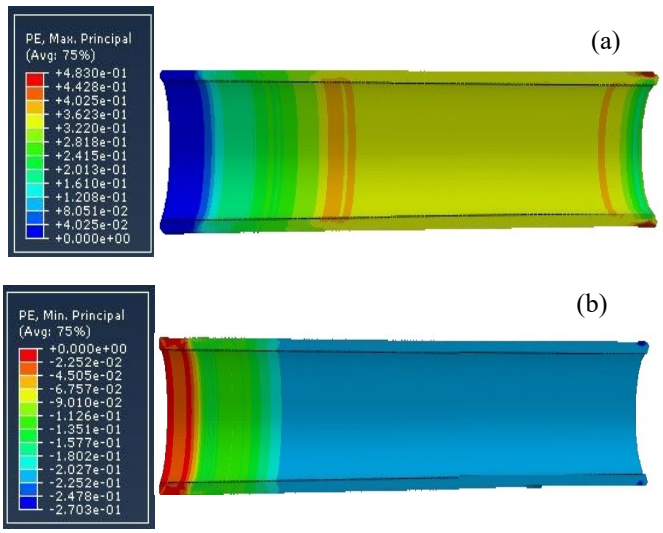

Fig. 7. Variations of principal strain (a) maximum and (b) minimum on AISI 410 steel tube during same cold drawing processes as section 2.1.

The stress distribution on the inner and outer surfaces of the tube is shown in Fig. 9 for different values of the half die angle. According to the findings of Kuboki [19], the residual stress after drawing is tensile on the outer surface and compressive on the inner surface. This finding can be seen in Fig. 9. It can be observed that the amount of residual stress in the tube increases with the decrease of the die angle. The lowest residual stress value was obtained at the half die angle of 16°. This value is associated with the optimal amount of friction and excess work applied. At the half die angle of 12 °, the friction increases and at the half die angle of 14 °, the effect of increasing redundant strain elevates the amount of the residual strains.

Fig. 10 shows the drawing force predicted by FEM for three different half die angles. The force increases at the die entrance, fluctuates steadily during the drawing, and finally decreases towards the end of the process. As expected, the lowest drawing force for half die angle of 16° was calculated to be about 164593 N. Half angles of 12° and 14°, produced forces of 168822 N and 165010 N, respectively (Fig. 9). The variations of drawing force revealed that at the beginning of deformation the applied force increases which is mainly due to the effects of friction, redundant strain and work hardening of the material. At the half-die angle of 16°, the consumption of deformation energy is at its

minimum which in turn results in optimum behavior of friction and redundant strain. Similar behavior was reported by Chobaut et al. [6], Palengat et al. [7], and Boutnel et al. [8]. When the half die angle is low, the drawing force rises since friction between surface of the tube and the die increases. Consequently, the maximum force needed for drawing is observed at the half die angle of 12°. Likewise, increase of the half die angle, results in augmentation of the drawing force due to the excessive amounts of redundant strain and work hardening of the material.

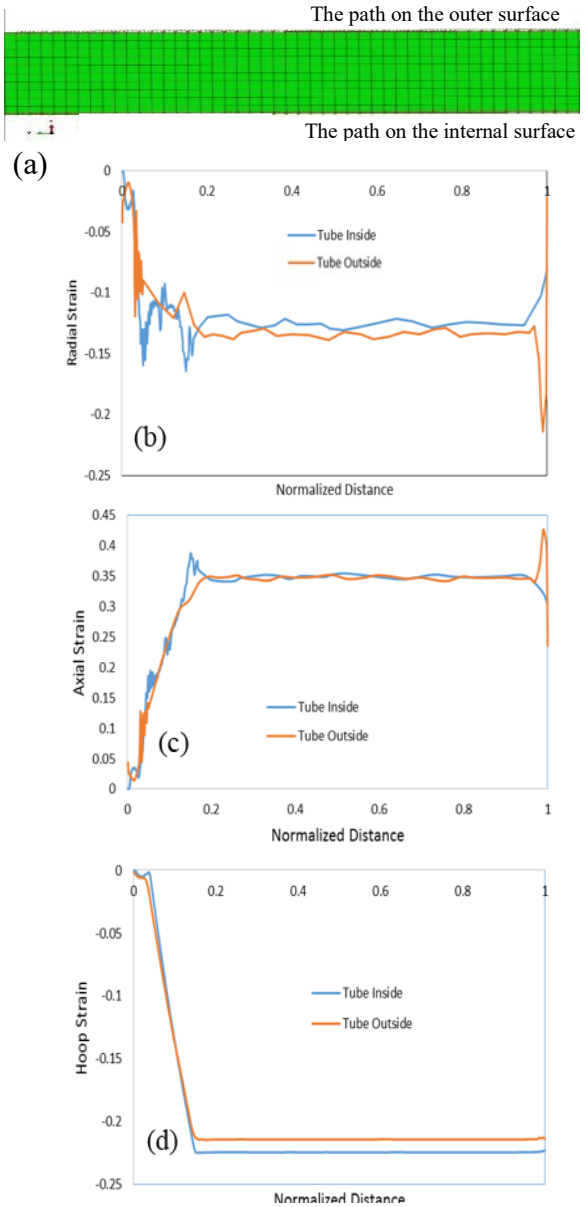

Fig. 8. Variations in values of (a) defined path, (b) radial, (c) axial, and (d) circumferential strain on internal and external surfaces along the length of the tube with friction coefficient of 0.15.

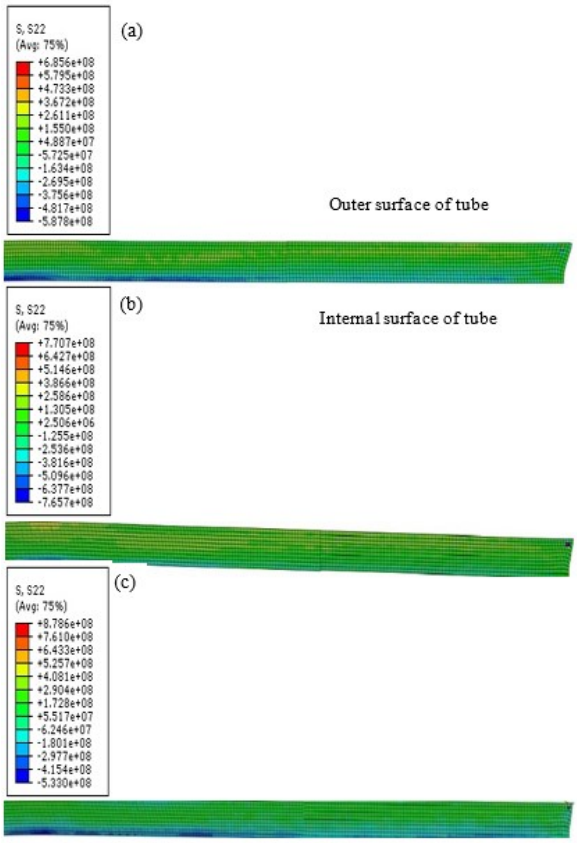

Fig. 9. Variation of internal and external surface stresses on the half die angles of (a) 16°, (b) 14°, and (c) 12° with a friction coefficient of 0.15.

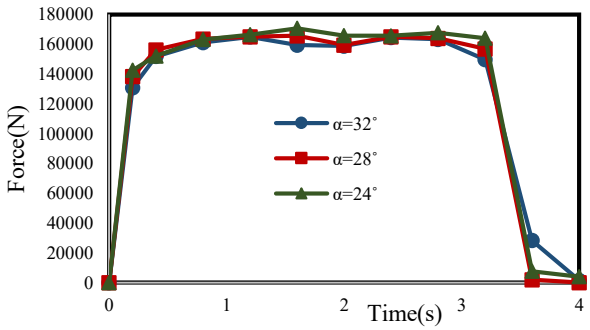

Fig. 10. Force variations during cold drawing process using three different half die angles.

3.2. Lower bound and upper bound approaches

It is very well known that the drawing force can be determined by different methods. Each of these approaches has its own characteristics. The application of lower bound theories for calculating the drawing force usually does not take into account the temperature and work hardening behavior of the material. On the other hand, in the upper bound method, the upper force limit

is predicted by considering the effects of work-hardening and redundant strains. At different half-die angles of 12°, 14° and 16° drawing force values were obtained by methods of lower and upper bound analysis as well as the FEM approach. As shown in Fig. 11, the results of applying the simulation method to calculate the drawing force is between the lower and upper bound theories. Moreover, as shown in Fig. 11, the lowest force required for drawing is at the half die angle of 16° for all theories. Using slab analysis, the calculated drawing force is 76077 N, 71593 N, and 68004 N for the half-die angles 12°, 14°, and 16°, respectively. The upper bound method gave a drawing force of 245000 N for the half angle of 16°.

According to the results of the FEM method a good prediction of the drawing force at the half die angle of 16° is obtained. The acquired simulation force was greater than the slab analysis but less than the upper bound analysis. The anticipated low value of force in the slab method is mainly due to overlooking the effects of work hardening and redundant strains.

3.3. Experimental results

By using equations 1 and 2, the practical force is calculated via the average value of electrical current during the drawing process. For the half die angle of 16°, the average electrical current was 49 A during drawing with the voltage of 380 V. The speed of drawing was about 0.08 m/s, i=63/10, n=2, r=0.1m, η_j=0.94. According to this data, ω and T_m were calculated to be 5.04 rad/s and 2955.55 N.m, respectively. Finally, according to engaged pairs of gears in the gearbox, the drawing force was found to be 175195 N (eq. 2). Table 2 shows the amounts of the actual drawing force with calculated forces using different methods of analysis. It can be seen that the predicted drawing force by simulation shows a better agreement with the actual drawing force with less than 7% variance.

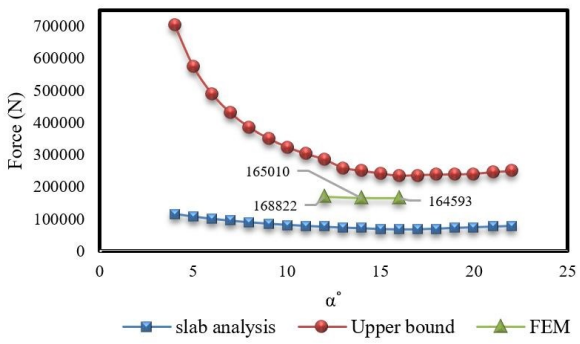

Fig. 11. Variations of drawing force for different half die angles using lower and upper bound analysis as well as FEM approach.

Table 2. Drawing force comparison in different methods (half-die angle16°)

Force (N)	Method
68004	Slab analysis
245000	Upper bound
175195	Experimental
164593	FEM

4. Conclusion

In this research different approaches of theoretical and simulation analysis were used to determine the optimum cold drawing force of a AISI 410 stainless steel tube in the drawing process. A fixed plug was used for this purpose and the effects of different parameters were evaluated. The following conclusions are reached:

- The drawing process of the samples were successfully performed using oxalate and soap lubricants. The friction coefficient was 0.15.
- Drawing oil, augmented the coefficient of friction and is not suitable for drawing of this steel.
- Using drawing experiments and Johnson-cock relations, a constitutive equation was suggested to explain the material flow behavior during the drawing process.
- In comparison with slab and upper bound analysis, simulating the process gave a more reasonable result to predict the required force.
- Circumferential strain has a considerable effect on the flow behavior of the steel. The maximum value of radial strain occurred at a half-die angle of 16 degrees.
- The lowest values of residual stresses occurred at the optimal half-die angle of 16 degrees.

Acknowledgments

The authors would like to sincerely thank Sepahan Rolling Tube and Profile (SRTP) Company for funding and supplying the materials used in this study.

Conflict of Interests

The authors declare no conflict of interest in this research.

5. References

[1] M. Hatala, F. Botko, J. Peterka, P. Bella and P. Radic, Evaluation of strain in cold drawing of tubes with internally shaped surface, *Materials Today: Proceedings, 22 (2)* (2020) 287-292.

[2] T. Furushima, T. Kishimoto, Achieving thin wall and high surface quality of magnesium alloy tubes in combined process of hollow sinking after die-less mandrel drawing, *International Journal of Material Forming,* 29 (2023).

[3] M. Jafari, M. Hosseinzadeh. M. Elyasi, Optimization of tube drawing process through FE analysis, intelligent computation, and experimental verification, *Journal of Process Mechanical Engineering*, 232 (1) (2018) 94-107.

[4] L. Donati, B. Reggiani, R. Pelaccia, M. Negozio, S. Di Donato, Advancements in extrusion and drawing: a review of the contributes by the ESAFORM community, *International Journal of Material Forming,* 41 (2022).

[5] J.M. Dreze, N. Chobaut, Mischle, Miniaturized tube fixed plug drawing: Determination of the friction coefficients and drawing limit of 316 LVM stainless steel, *Journal of Materials Processing Tech*, 263 (2019) 396-407.

[6] M. Palengat, G. Chagnon, D. Favier, H. Louche, C. Linardon, C. Plaideau, Cold drawing of 316l stainless steel thin-walled tubes: experiments and finite element analysis, *International Journal of Mechanical Sciences*, 70 (2013) 69–78.

[7] N.C. Linardon, D. Favier, B. Gruez, A conical mandrel tube drawing test designed to assess failure criteria, *Journal of Materials Processing Tec,* 214 (2014) 347-357.

[8] F. Boutenel, M. Delhommeb, V. Velay, B. Boman, Finite element modelling of cold drawing for high-precision tubes, *Comptes Rendus Mécanique,* 346 (2018) 665–677.

[9] M. Nekpal, M. Martinkovič, Determination of the coefficient of friction under cold tube drawing using FEM simulation and drawing force measurement, *Research Papers Faculty of Materials Science and Technology Slovak University of Technology,* 26 (2018) 29-34.

[10] J. Gattmah, F. Ozturk, S. Orhan, Effects of the semi die/plug angles on cold tube drawing with a fixed plug by FEM for AISI 1010 steel tube, *Published in 4th International Symposium on Innovative Technologies in Engineering and Science,* 21 (2016) 886-892.

[11] J.F. Beland, M. Fafard, A. D. Rahem, G. Amours, T. Cote, Optimization on the cold drawing process of 6063 aluminium tubes, *Applied Mathematical Modelling,* 35(11) (2011) 5302-5313.

[12] K. Keun um, D. Nyung Lee, An upper bound solution of tube drawing, *Applied Mathematical Modelling,* 35(11) (2011) 5302-5313.

[13] R.L. Mott, E.M. Vavrek, J. Wang, Machine elements in mechanical design, *Pearson Education,* 6 (2018).

[14] G. R. Johnson, W. H. Cook, A constitutive model and data for metals subjected to large strains, high strain rates and high temperatures, *Proceedings of the 7th International Symposium on Ballistics, (*1983) 541-547.

[15] K. Limbadri, H.N. Krishnamurthy, A. Maruthi Ram, N. Saibaba, Development of Johnson-Cook model for zircaloy-4 with low oxygen content, *Materials Today: Proceedings*, 4 (2017) 966-974.

[16] E. Eduardo, J. Cabezas, Celentan, Experimental and numerical analysis of the tensile test using sheet specimens, *Finite Elements in Analysis and Design,* 40 (2004) 555-575.

[17] W. Hosford, F. Caddle, Metal Forming Mechanics and Metallurgy, Cambridge University Press, New York, 2011.

[18] B. Avitzur, C. J. Van Tyne, Ring forming: An upper bound approach, *J. Eng. Ind. Trans. ASME*, 104 (1982) 231-252.

[19] T. Kuboki, K. Nishida, T. Sakaki, M. Murata, Effect of plug on levelling of residual stress in tube drawing, *Journal of Materials Processing Technology,* 204 (2008) 162-168.